

Neutron star properties in density-dependent relativistic Hartree-Fock theory

Bao Yuan Sun (孙保元),¹ Wen Hui Long (龙文辉),^{1,2} Jie Meng (孟杰),^{1,3,4,5} and U. Lombardo^{6,7}
¹*School of Physics and State Key Laboratory of Nuclear Physics and Technology, Peking University, 100871 Beijing, People's Republic of China*

²*Physik-Department der Technischen Universität München, D-85748 Garching, Germany*

³*Department of Physics, University of Stellenbosch, Stellenbosch, South Africa*

⁴*Institute of Theoretical Physics, Chinese Academy of Sciences, 100080 Beijing, People's Republic of China*

⁵*Center of Theoretical Nuclear Physics, National Laboratory of Heavy Ion Accelerator, 730000 Lanzhou, People's Republic of China*

⁶*Laboratori Nazionali del Sud, Istituto Nazionale di Fisica Nucleare, Via S. Sofia 62, I-95123 Catania, Italy*

⁷*Dipartimento di Fisica e Astronomia, Università di Catania, viale Andrea Doria 6, I-95125 Catania, Italy*

(Received 7 October 2008; published 31 December 2008)

With the equations of state provided by the newly developed density-dependent relativistic Hartree-Fock (DDRHF) theory for hadronic matter, the properties of the static and β -equilibrium neutron stars without hyperons are studied for the first time and compared to the predictions of the relativistic mean-field models and recent observational data. The influences of Fock terms on properties of asymmetric nuclear matter at high densities are discussed in detail. Because of the significant contributions from the σ - and ω -exchange terms to the symmetry energy, large proton fractions in neutron stars are predicted by the DDRHF calculations, which strongly affect the cooling process of the star. A critical mass of about $1.45M_{\odot}$, close to the limit of $1.5M_{\odot}$ determined by modern soft X-ray data analysis, is obtained by DDRHF with the effective interactions PKO2 and PKO3 for the occurrence of the direct Urca process in neutron stars. The maximum masses of neutron stars given by the DDRHF calculations lie between $2.45M_{\odot}$ and $2.49M_{\odot}$, which are in reasonable agreement with the high pulsar mass of $(2.08 \pm 0.19)M_{\odot}$ from PSR B1516 + 02B. It is also found that the mass-radius relations of neutron stars determined by DDRHF are consistent with the observational data from thermal radiation measurements in the isolated neutron star RX J1856, quasiperiodic brightness oscillations in the low-mass X-ray binaries 4U 0614 + 09 and 4U 1636-536, and the redshift determined in the low-mass X-ray binary EXO 0748-676.

DOI: [10.1103/PhysRevC.78.065805](https://doi.org/10.1103/PhysRevC.78.065805)

PACS number(s): 21.30.Fe, 21.60.Jz, 21.65.-f, 26.60.-c

I. INTRODUCTION

The investigative territory of nuclear physics has been enormously expanded with the construction of new accelerator facilities as well as the development of land- and space-based observatories. The exploration over the phase diagram of matter has been extended to the extreme conditions of density, pressure, and temperature during the past several decades, and is now one of the hottest topics in both theoretical and experimental nuclear physics. Around saturation density nuclear matter properties can be well calibrated by terrestrial experiments with atomic nuclei, but neutron stars are the natural laboratories in the universe for exploring the equation of state (EoS) of baryonic matter at low temperature and higher baryonic densities [1–3]. In addition, probing the elliptical flow and kaon production in heavy-ion collisions provides extra information for the nuclear EoS at high temperature and about 2–4.5 times nuclear saturation density [4–6].

As some of the most exotic objects in the universe, neutron stars play the role of a bridge between nuclear physics and astrophysics. With the discovery of the neutron in 1932, the concept of the neutron star were first proposed by Landau [7]. Two years later, the neutron star was deemed to be formed in *supernovae* [8]. In the 1960s, the observed radio pulsars [9] were identified as rotating neutron stars [10]. Currently, the neutron star is generally considered to have a crustal structure [11]. Below the atmosphere and envelope surface, which have negligible mass, the crust extends about 1 to 2 km into the star, which mainly consists of nuclei and free

electrons. With increasing density, the dominant nuclei in the crust vary from ^{56}Fe to extremely neutron-rich nuclei, and neutrons may gradually leak out of nuclei to form the neutron fluid. The outer core ($\rho \gtrsim \rho_0/3$) of neutron stars is composed of a soup of nucleons, electrons, and muons. In the inner core, exotic particles—such as the strangeness-bearing hyperons and/or Bose condensates (pions or kaons)—may become abundant, and a transition to a mixed phase of hadronic and deconfined quark matter becomes possible. Although similar equations of state at saturation and subsaturation densities are obtained by various nuclear matter models, their deviations are very remarkable in the high-density region, which is very essential in describing and predicting the properties of neutron stars. Further investigations are therefore necessitated for the detailed structure over the density range of neutron stars.

The recent observations of neutron stars have been extensively reviewed (see, e.g., Ref. [12]). The existence of massive compact stars of $2M_{\odot}$ or above is now unveiled by some evidence. Careful analysis of the *Rossi X-ray Timing Explorer (RXTE)* data for the quasiperiodic brightness oscillations (QPOs) discovered from the low-mass X-ray binaries (LMXBs) 4U 1636-536 shows that several neutron stars in LMXBs have gravitational masses between $1.9M_{\odot}$ and possibly $2.1M_{\odot}$ [13]. Measurements on millisecond pulsars in globular cluster NGC 5904 (M5) during 19 years of Arecibo timing yield $M = (2.08 \pm 0.19)M_{\odot}$ for PSR B1516 + 02B [14], whereas a much larger pulsar mass of $(2.74 \pm 0.21)M_{\odot}$ was presented very recently for PSR J1748-2021B in NGC 6440 [15]. Besides the maximum mass limits, the mass-radius

relation is also constrained by the recent observations. The thermal radiation spectra in X rays and in optical-UV from the isolated neutron star RX J1856.5-3754 (or RX J1856 for short) determine the large radiation radius R_∞ as 16.8 km [16]. The model fitting to the high-quality X-ray spectrum of the quiescent LMXB X7 in the globular cluster 47 Tuc prefers a rather large radius of $14.5^{+1.8}_{-1.6}$ km for a $1.4M_\odot$ compact star [17]. In another LMXB, EXO 0748-676, a pair of resonance scattering lines consistent with Fe XXV and XXVI gives a redshift z of about 0.345, which constrains the mass to $M \geq (2.10 \pm 0.28)M_\odot$ and the radius to $R \geq 13.8 \pm 1.8$ km for the same object [18,19]. In addition, the highest QPO frequency of 1330 Hz ever observed in 4U 0614 + 09 implies a mass $M \lesssim 1.8M_\odot$ and a radius $R \lesssim 15$ km in this object [20]. Furthermore, modern observational soft X-ray data of cooling neutron stars associated with popular synthesis model analyses reveal that an acceptable EoS does not allow the direct Urca process [21] to occur in neutron stars with masses below $1.5M_\odot$ [22–24]. All of these indicate the strict constraints on the EoS of strongly interacting matter at high densities.

For the description of nuclear matter and finite nuclei, the relativistic many-body theory has achieved great success during the past years. One of the most successful representatives is the relativistic Hartree approach with the no-sea approximation, namely the relativistic mean-field (RMF) theory [25–27]. With a limited number of free parameters including the meson masses and meson-nucleon coupling constants, the appropriate quantitative descriptions are obtained by RMF for both stable nuclei and exotic ones with large neutron excess [28–41].

After the first theoretical calculations of the neutron star properties [42,43], plenty of theoretical predictions were presented using both nonrelativistic and relativistic approaches in the literature. In the early development of RMF, it was applied to evaluate the total mass and radius of neutron stars [44]. In its further development, nuclear medium effects were taken into account by introducing the explicit or implicit density dependence into the meson-nucleon couplings (i.e., the density-dependent meson-nucleon couplings [45–47] and the nonlinear self-couplings of the meson fields [39,48,49], respectively). In Refs. [48,50,51], the effects of the nonlinear self-coupling of σ , ω , and ρ mesons were studied in describing nuclear matter and neutron stars. On the other side, the influence on mean-field potentials, saturation properties of nuclear matter, the EoS, and the maximum mass and radius of neutron stars was systematically investigated with explicit density dependence in the meson-nucleon couplings [52,53]. In addition, the consequences on compact star properties were studied with the inclusion of the degree of freedom of hyperons [54–57]. With more accurate experimental data of the neutron radius of ^{208}Pb , the correlation between the neutron skin thickness in finite nuclei and the symmetry energy of nuclear matter was discussed [58–60]. In further investigation in Ref. [61] it was proposed that neutron stars with larger neutron star radii had thicker neutron skins, which implies constraints on the EoS and on the cooling mechanism of neutron stars. Besides the RMF approach, the Dirac-Brueckner-Hartree-Fock (DBHF) and Brueckner-Hartree-Fock (BHF) with three-body force approaches were

also applied to study neutron star properties with realistic nucleon-nucleon interactions [62–66].

In the RMF approach, however, the Fock terms are neglected for simplicity. From the recent development of the relativistic Hartree-Fock theory, that is, the density-dependent relativistic Hartree-Fock (DDRHF) theory [67], it is found that the Fock terms are of special importance in determining the nuclear structure properties. Within DDRHF, quantitatively comparable precision with RMF is obtained for the structure properties of nuclear matter and finite nuclei [67,68]. Particularly, the new constituents introduced with the Fock terms (i.e., the ρ -tensor correlations and pion exchange potential) have brought significant improvement to the descriptions of the nuclear shell structures [68] and their evolution [69]. Furthermore, the excitation properties and the non-energy-weighted sum rules of the Gamow-Teller resonance and the spin-dipole resonance in doubly magic nuclei have been well reproduced by the random-phase approximation (RPA) based on the DDRHF approach fully self-consistently [70]. Since nuclear structure properties around the saturation density are evidently affected by the Fock terms, one might expect remarkable effects from the Fock terms on nuclear matter properties in the high-density region. Especially with the inclusion of the new ingredients in DDRHF, remarkable adjustment occurs on the coupling strength of the dominant mean fields (g_σ and g_ω), which may bring significant effects when exploring the high-density region.

In this paper, the properties of the static and β -equilibrium neutron stars without hyperons are studied within the DDRHF theory. As compared to the calculations of the RMF theory, the applicable ranges of density and isospin asymmetry are tested for DDRHF as well as for consistency with recent observational constraints of compact stars. Section II briefly introduces the formalism of DDRHF for nuclear matter and neutron stars. In Sec. III, the calculated results and discussions are given, including the properties of symmetric and asymmetric nuclear matter in comparison with RMF in Sec. III A, in which the effects of Fock terms are studied in detail, and the investigations of neutron stars in comparison with recent observational data in Sec. III B. Finally a summary is given in Sec. IV.

II. GENERAL FORMULISM OF DENSITY-DEPENDENT RELATIVISTIC HARTREE-FOCK THEORY IN NUCLEAR MATTER

The relativistic Hartree-Fock (RHF) theory with density-dependent meson-nucleon couplings (i.e., the DDRHF theory) was first introduced in Ref. [67], and the applications and corresponding effective interactions can be found in Refs. [67–69,71]. In the following we just briefly recall the general formalism of DDRHF in nuclear matter and the application in neutron stars. For more details of the RHF theory we refer the reader to Refs. [67,68,72].

As the theoretical starting point, the Lagrangian density of DDRHF is constructed on the one-boson exchange diagram of the NN interaction, which contains the degrees of freedom associated with the nucleon (ψ), two isoscalar mesons (σ and

ω), two isovector mesons (π and ρ), and the photon (A). Following the standard procedure in Ref. [72], one can derive the Hamiltonian in nucleon space as

$$H = \int d^3x \bar{\psi}(-i\boldsymbol{\gamma} \cdot \nabla + M)\psi + \frac{1}{2} \int d^3x d^4y \sum_{\phi} \bar{\psi}(x) \bar{\psi}(y) \Gamma_{\phi}(1, 2) D_{\phi}(1, 2) \psi(y) \psi(x), \quad (1)$$

where $\phi = \sigma, \omega, \rho, \pi$, and A , and D_{ϕ} denotes the propagators of mesons and photons. The interacting vertex Γ_{ϕ} in the Hamiltonian (1) is

$$\Gamma_{\sigma}(1, 2) \equiv -g_{\sigma}(1)g_{\sigma}(2), \quad (2a)$$

$$\Gamma_{\omega}(1, 2) \equiv +g_{\omega}(1)\gamma_{\mu}(1)g_{\omega}(2)\gamma^{\mu}(2), \quad (2b)$$

$$\Gamma_{\rho}(1, 2) \equiv +g_{\rho}(1)\gamma_{\mu}(1)\vec{\tau}(1) \cdot g_{\rho}(2)\gamma^{\mu}(2)\vec{\tau}(2), \quad (2c)$$

$$\Gamma_{\pi}(1, 2) \equiv -\frac{1}{m_{\pi}^2} [f_{\pi} \vec{\tau} \gamma_5 \boldsymbol{\gamma} \cdot \nabla]_1 \cdot [f_{\pi} \vec{\tau} \gamma_5 \boldsymbol{\gamma} \cdot \nabla]_2, \quad (2d)$$

$$\Gamma_A(1, 2) \equiv +\frac{e^2}{4} [\gamma_{\mu}(1 - \tau_3)]_1 [\gamma^{\mu}(1 - \tau_3)]_2. \quad (2e)$$

In the current work, the ρ -tensor correlations are not enclosed. In these expressions and in the following context, the isovectors are denoted by arrows and the space vectors are in bold type.

In general, the time component of the four-momentum carried by mesons is neglected on the level of the mean-field approximation. This neglect has no consequence on the direct (Hartree) terms, but for the exchange (Fock) terms it amounts to neglecting retardation effects. The meson propagators are therefore of the Yukawa form, for example, in the momentum representation,

$$D_{\phi}(1, 2) = \frac{1}{m_{\phi}^2 + \mathbf{q}^2}, \quad (3)$$

where the exchanging momentum is $\mathbf{q} = \mathbf{p}_2 - \mathbf{p}_1$ and $\phi = \sigma, \omega, \rho$, and π .

For the description of nuclear matter, the coulomb field thus could be neglected, and the momentum representation is generally adopted in the Hamiltonian. Because of time-reversal symmetry and rotational invariance, the self-energy Σ can be expressed as

$$\Sigma(p) = \Sigma_S(p) + \gamma_0 \Sigma_0(p) + \boldsymbol{\gamma} \cdot \hat{\mathbf{p}} \Sigma_V(p), \quad (4)$$

where $\hat{\mathbf{p}}$ is the unit vector along \mathbf{p} , and the scalar component Σ_S , time component Σ_0 , and space component Σ_V of the vector potential are functions of the four-momentum $p = [E(p), \mathbf{p}]$ of the nucleon. With the general form of the self-energy, the Dirac equation in nuclear matter can be written as

$$(\boldsymbol{\gamma} \cdot \mathbf{p}^* + M^*) u(p, s, \tau) = \gamma_0 E^* u(p, s, \tau), \quad (5)$$

with the starred quantities

$$\mathbf{p}^* = \mathbf{p} + \hat{\mathbf{p}} \Sigma_V(p), \quad (6a)$$

$$M^* = M + \Sigma_S(p), \quad (6b)$$

$$E^* = E(p) - \Sigma_0(p), \quad (6c)$$

which obey the relativistic mass-energy relation $E^{*2} = \mathbf{p}^{*2} + M^{*2}$. With this relationship, one can introduce the hatted quantities as

$$\hat{P} \equiv \frac{\mathbf{p}^*}{E^*}, \quad \hat{M} \equiv \frac{M^*}{E^*}. \quad (7)$$

With the momentum representation, the Dirac equation (5) can be formally solved and the Dirac spinors with positive energy are

$$u(p, s, \tau) = \left[\frac{E^* + M^*}{2E^*} \right]^{1/2} \begin{pmatrix} 1 \\ \frac{\boldsymbol{\sigma} \cdot \mathbf{p}^*}{E^* + M^*} \end{pmatrix} \chi_s \chi_{\tau}, \quad (8)$$

where χ_s and χ_{τ} , respectively, denote the spin and isospin wave functions. The solution of the Dirac Eq. (5) is normalized as

$$u^{\dagger}(p, s, \tau) u(p, s, \tau) = 1. \quad (9)$$

The stationary solutions of the Dirac equation (5) consist of the positive and negative energy ones, and one can expand the nucleon field operator ψ in terms of Dirac spinors. Within the mean-field approximation, the contributions from the negative-energy states are neglected (i.e., the no-sea approximation). The nucleon field operator ψ is therefore expanded on the positive-energy set as

$$\psi(x) = \sum_{p,s,\tau} u(p, s, \tau) e^{-ipx} c_{p,s,\tau}, \quad (10a)$$

$$\psi^{\dagger}(x) = \sum_{p,s,\tau} u^{\dagger}(p, s, \tau) e^{ipx} c_{p,s,\tau}^{\dagger}, \quad (10b)$$

where $c_{p,s,\tau}$ and $c_{p,s,\tau}^{\dagger}$ are the annihilation and creation operators. With the no-sea approximation, the trial Hartree-Fock ground state can be constructed as

$$|\Phi_0\rangle = \prod_{p,s,\tau} c_{p,s,\tau}^{\dagger} |0\rangle, \quad (11)$$

where $|0\rangle$ is the vacuum state. The energy functional (i.e., the energy density in nuclear matter) is then obtained by taking the expectation of the Hamiltonian with respect to the ground state $|\Phi_0\rangle$ in a given volume Ω ,

$$\begin{aligned} \varepsilon &= \frac{1}{\Omega} \langle \Phi_0 | H | \Phi_0 \rangle \equiv \langle T \rangle + \sum_{\phi} \langle V_{\phi} \rangle \\ &= \varepsilon_k + \sum_{\phi} (\varepsilon_{\phi}^D + \varepsilon_{\phi}^E), \end{aligned} \quad (12)$$

where $\phi = \sigma, \omega, \rho, \pi$ and

$$\varepsilon_k = \sum_{p,s,\tau} \bar{u}(p, s, \tau) (\boldsymbol{\gamma} \cdot \mathbf{p} + M) u(p, s, \tau), \quad (13a)$$

$$\begin{aligned} \varepsilon_{\phi}^D &= \frac{1}{2} \sum_{p_1, s_1, \tau_1} \sum_{p_2, s_2, \tau_2} \bar{u}(p_1, s_1, \tau_1) \bar{u}(p_2, s_2, \tau_2) \Gamma_{\phi}(1, 2) \\ &\quad \times \frac{1}{m_{\phi}^2} u(p_2, s_2, \tau_2) u(p_1, s_1, \tau_1), \end{aligned} \quad (13b)$$

$$\begin{aligned} \varepsilon_{\phi}^E &= -\frac{1}{2} \sum_{p_1, s_1, \tau_1} \sum_{p_2, s_2, \tau_2} \bar{u}(p_1, s_1, \tau_1) \bar{u}(p_2, s_2, \tau_2) \Gamma_{\phi}(1, 2) \\ &\quad \times \frac{1}{m_{\phi}^2 + \mathbf{q}^2} u(p_1, s_1, \tau_1) u(p_2, s_2, \tau_2). \end{aligned} \quad (13c)$$

In the energy functional, ε_k denotes the kinetic energy density, and ε_ϕ^D and ε_ϕ^E , respectively, correspond to the direct (Hartree) and exchange (Fock) terms of the potential energy density. With the Dirac spinors in Eq. (8), one can obtain the contributions of the energy density from each channel. The kinetic energy density ε_k and the direct terms of the potential energy density ε_ϕ^D can be written as

$$\varepsilon_k = \sum_{i=n,p} \frac{1}{\pi^2} \int_0^{k_{F,i}} p^2 dp (p \hat{P} + M \hat{M}), \quad (14a)$$

$$\varepsilon_\sigma^D = -\frac{1}{2} \frac{g_\sigma^2}{m_\sigma^2} \rho_s^2, \quad (14b)$$

$$\varepsilon_\omega^D = +\frac{1}{2} \frac{g_\omega^2}{m_\omega^2} \rho_b^2, \quad (14c)$$

$$\varepsilon_\rho^D = +\frac{1}{2} \frac{g_\rho^2}{m_\rho^2} \rho_{b3}^2, \quad (14d)$$

where the scalar density ρ_s , baryonic density ρ_b , and the third component ρ_{b3} are

$$\rho_s = \sum_{i=n,p} \frac{1}{\pi^2} \int_0^{k_{F,i}} p^2 dp \hat{M}(p), \quad (15a)$$

$$\rho_b = \sum_{i=n,p} \frac{k_{F,i}^3}{3\pi^2}, \quad (15b)$$

$$\rho_{b3} = \frac{k_{F,n}^3}{3\pi^2} - \frac{k_{F,p}^3}{3\pi^2}, \quad (15c)$$

with the Fermi momentum $k_{F,i}$ ($i = n, p$).

Compared to the simple form of direct terms of the potential energy density, the exchange terms are much more complicated. In the isoscalar channels ($\phi = \sigma, \omega$), the expressions read as

$$\varepsilon_\phi^E = \frac{1}{2} \frac{1}{(2\pi)^4} \sum_{\tau, \tau'} \delta_{\tau\tau'} \int pp' dp dp' [A_\phi(p, p') + \hat{M}(p) \hat{M}(p') B_\phi(p, p') + \hat{P}(p) \hat{P}(p') C_\phi(p, p')]. \quad (16)$$

For the isovector channels ($\phi = \rho, \pi$), one just needs to replace the isospin factor $\delta_{\tau\tau'}$ by $(2 - \delta_{\tau\tau'})$ in this expression. The details of the terms A_ϕ , B_ϕ , and C_ϕ in Eq. (16) are shown in Table I, where the functions $\Theta_\phi(p, p')$ and $\Phi_\phi(p, p')$ are

defined as

$$\int d\Omega d\Omega' \frac{1}{m_\phi^2 + q^2} = \frac{4\pi^2}{pp'} \ln \frac{m_\phi^2 + (p + p')^2}{m_\phi^2 + (p - p')^2} \equiv \frac{4\pi^2}{pp'} \Theta_\phi(p, p'), \quad (17a)$$

$$\int d\Omega d\Omega' \frac{\hat{p} \cdot \hat{p}'}{m_\phi^2 + q^2} = \frac{4\pi^2}{pp'} \left\{ \frac{p^2 + p'^2 + m_\phi^2}{2pp'} \Theta_\phi(p, p') - 2 \right\} \equiv 2 \frac{4\pi^2}{pp'} \Phi_\phi(p, p'). \quad (17b)$$

From the potential energy densities in Eqs. (13b) and (13c), one can perform the following variation:

$$\Sigma(p)u(p, s, \tau) = \frac{\delta}{\delta \bar{u}(p, s, \tau)} \sum_{\sigma, \omega, \rho, \pi} [\varepsilon_\phi^D + \varepsilon_\phi^E] \quad (18)$$

and obtain the self-energy $\Sigma(p)$, which includes the direct terms

$$\Sigma_S^D = -\frac{g_\sigma^2}{m_\sigma^2} \rho_s, \quad (19a)$$

$$\Sigma_0^D = +\frac{g_\omega^2}{m_\omega^2} \rho_b + \frac{g_\rho^2}{m_\rho^2} \rho_{b3} \quad (19b)$$

and the exchange terms

$$\Sigma_{\tau, S}^E(p) = \frac{1}{(4\pi)^2 p} \int \hat{M}(p') p' dp' \sum_{\tau'} \{ \delta_{\tau\tau'} [B_\sigma + B_\omega]_{(p, p')} + (2 - \delta_{\tau\tau'}) [B_\rho + B_\pi]_{(p, p')} \}, \quad (20a)$$

$$\Sigma_{\tau, 0}^E(p) = \frac{1}{(4\pi)^2 p} \int p' dp' \sum_{\tau'} \{ \delta_{\tau\tau'} [A_\sigma + A_\omega]_{(p, p')} + (2 - \delta_{\tau\tau'}) [A_\rho + A_\pi]_{(p, p')} \}, \quad (20b)$$

$$\Sigma_{\tau, V}^E(p) = \frac{1}{(4\pi)^2 p} \int \hat{P}(p') p' dp' \sum_{\tau'} \{ \delta_{\tau\tau'} [C_\sigma + C_\omega]_{(p, p')} + (2 - \delta_{\tau\tau'}) [C_\rho + C_\pi]_{(p, p')} \}. \quad (20c)$$

In DDRHF, the explicit density dependence is introduced into the meson-nucleon couplings (i.e., the coupling constants $g_\sigma, g_\omega, g_\rho$, and f_π are functions of the baryonic density ρ_b). In the isoscalar meson-nucleon coupling channels, one has the following form:

$$g_\phi(\rho_b) = g_\phi(\rho_0) f_\phi(x), \quad (21)$$

TABLE I. The terms A_ϕ , B_ϕ , and C_ϕ in Eq. (16).

ϕ	$A_\phi(p, p')$	$B_\phi(p, p')$	$C_\phi(p, p')$
σ	$g_\sigma^2 \Theta_\sigma(p, p')$	$g_\sigma^2 \Theta_\sigma(p, p')$	$-2g_\sigma^2 \Phi_\sigma(p, p')$
ω	$2g_\omega^2 \Theta_\omega(p, p')$	$-4g_\omega^2 \Theta_\omega(p, p')$	$-4g_\omega^2 \Phi_\omega(p, p')$
ρ	$2g_\rho^2 \Theta_\rho(p, p')$	$-4g_\rho^2 \Theta_\rho(p, p')$	$-4g_\rho^2 \Phi_\rho(p, p')$
π	$-f_\pi^2 \Theta_\pi(p, p')$	$-f_\pi^2 \Theta_\pi(p, p')$	$2 \frac{f_\pi^2}{m_\pi^2} [(p^2 + p'^2) \Phi_\pi(p, p') - pp' \Theta_\pi(p, p')]$

where $x = \rho_b/\rho_0$ with ρ_0 the saturation density of nuclear matter, and the function f_ϕ is

$$f_\phi(x) = a_\phi \frac{1 + b_\phi(x + d_\phi)^2}{1 + c_\phi(x + d_\phi)^2}. \quad (22)$$

In addition, five constraints, $f''_\sigma(1) = f''_\omega(1)$, $f_\phi(1) = 1$, and $f''_\phi(0) = 0$ ($\phi = \sigma, \omega$), are introduced to reduce the number of free parameters. For the isovector channels, the exponential density dependence is adopted for g_ρ and f_π :

$$g_\rho(\rho_b) = g_\rho(0) e^{-a_\rho x}, \quad (23)$$

$$f_\pi(\rho_b) = f_\pi(0) e^{-a_\pi x}. \quad (24)$$

Because of the density dependence in meson-nucleon couplings, the additional contribution (i.e., the rearrangement term Σ_R) appears in the self-energy Σ . In nuclear matter, it can be written as

$$\Sigma_R = \sum_{\phi=\sigma,\omega,\rho,\pi} \frac{\partial g_\phi}{\partial \rho_b} \sum_\tau \frac{1}{\pi^2} \int [\hat{M}(p) \Sigma_{\tau,S}^\phi(p) + \Sigma_{\tau,0}^\phi(p) + \hat{P}(p) \Sigma_{\tau,V}^\phi(p)] p^2 dp. \quad (25)$$

From Eqs. (19), (20), and (25), the scalar component Σ_S , time component Σ_0 , and space component Σ_V of the vector potential in Eq. (4) can be obtained as

$$\Sigma_S(p) = \Sigma_S^D + \Sigma_S^E(p), \quad (26a)$$

$$\Sigma_0(p) = \Sigma_0^D + \Sigma_0^E(p) + \Sigma_R, \quad (26b)$$

$$\Sigma_V(p) = \Sigma_V^E(p), \quad (26c)$$

from which the starred quantities in Eq. (6) and the hatted quantities in Eq. (7) can be obtained. Therefore, for nuclear matter with given baryonic density ρ_b and neutron-proton ratio N/Z , one can proceed by a self-consistent iteration to investigate their properties: With the trial self-energies, one can determine the starred quantities and hatted quantities and calculate the scalar density, and then get the new self-energies for the next iteration until final convergence is obtained.

In this work, a neutron star is described as the β -stable nuclear matter system, which consists of not only neutrons and protons but also leptons λ (mainly e^- and μ^-). The equations of motion for the leptons are the free Dirac equations and their densities can be expressed in terms of their corresponding Fermi momenta, $\rho_\lambda = k_{F,\lambda}^3/(3\pi^2)$ ($\lambda = e^-, \mu^-$). The chemical potentials of nucleons and leptons satisfy the equilibrium conditions

$$\mu_p = \mu_n - \mu_e, \quad \mu_\mu = \mu_e, \quad (27)$$

where the chemical potentials μ_n , μ_p , μ_μ , and μ_e are determined by the relativistic energy-momentum relation at the momentum $p = k_F$,

$$\mu_i = \Sigma_0(k_{F,i}) + E^*(k_{F,i}), \quad (28a)$$

$$\mu_\lambda = \sqrt{k_{F,\lambda}^2 + m_\lambda^2}, \quad (28b)$$

where $i = n, p$ and $\lambda = e^-, \mu^-$. The lepton masses are, respectively, $m_e = 0.511$ MeV and $m_\mu = 105.658$ MeV. In addition, baryon density conservation and charge neutrality

are imposed as

$$\rho_b = \rho_n + \rho_p, \quad \rho_p = \rho_\mu + \rho_e. \quad (29)$$

With these constraints, the energy density of neutron stars is then obtained as

$$\varepsilon_{\text{ns}} = \sum_{i=n,p,e,\mu} \varepsilon_{k,i} + \sum_{\phi=\sigma,\omega,\rho,\pi} (\varepsilon_\phi^D + \varepsilon_\phi^E). \quad (30)$$

Here the leptons are treated as a free Fermi gas by assuming that there are no interactions between leptons and nucleons or mesons and the kinetic energies of leptons can be expressed as

$$\varepsilon_{k,\lambda} = \frac{1}{\pi^2} \int_0^{k_{F,\lambda}} p^2 dp \sqrt{p^2 + m_\lambda^2}. \quad (31)$$

With the thermodynamic relation, the pressure of the neutron star system can be obtained as

$$P(\rho_b) = \rho_b^2 \frac{d}{d\rho_b} \frac{\varepsilon_{\text{ns}}}{\rho_b} = \sum_{i=n,p,e,\mu} \rho_i \mu_i - \varepsilon_{\text{ns}}. \quad (32)$$

In the low-density region ($\rho_b < 0.08 \text{ fm}^{-3}$), instead of DDRHF calculations, the BPS [73] and BBP [74] models are chosen to provide the proper EoS.

The structure equations of a static, spherically symmetric, and relativistic star are the Tolman-Oppenheimer-Volkov (TOV) equations [42,43]. By taking $c = G = 1$, the TOV equations become

$$\frac{dP}{dr} = - \frac{[P(r) + \varepsilon(r)][M(r) + 4\pi r^3 P(r)]}{r[r - 2M(r)]}, \quad (33a)$$

$$\frac{dM}{dr} = 4\pi r^2 \varepsilon(r), \quad (33b)$$

where $P(r)$ is the pressure of the star at radius r , and $M(r)$ is the total star mass inside a sphere of radius r . Taking the equation of state of stellar matter as the input, one could proceed with the solution of TOV equations. The point R , at which the pressure vanishes [i.e., $P(R) = 0$] defines the radius of the star, and the corresponding $M(R)$ is the gravitational mass. For a given EoS, the TOV equation has the unique solution that depends on a single parameter characterizing the conditions of matter at the center, such as the central density $\rho(0)$ or the central pressure $P(0)$.

III. RESULTS AND DISCUSSION

In this paper, the EoS and the neutron star properties are studied in DDRHF with the effective interactions PKO1, PKO2, and PKO3 [67,69]. As shown in Table II, the coupling constant $g_\rho(0)$ is fixed to the value in the free space in PKO1, whereas it is free to be adjusted in PKO2 and PKO3, and π -coupling is not included in PKO2. For comparison, the results calculated by RMF are also discussed. The effective interactions used in RMF calculations include the nonlinear self-coupling ones GL-97 [44], NL1 [75], NL3 [37], NLSH [76], TM1 [49], and PK1 [39] and the density-dependent ones TW99 [38], DD-ME1 [40], DD-ME2 [41], and PKDD [39].

TABLE II. The effective interactions PKO1, PKO2, and PKO3 of DDRHF [67], where the masses are $M = 938.9$ MeV, $m_\omega = 783.0$ MeV, $m_\rho = 769.0$ MeV, and $m_\pi = 138.0$ MeV.

	m_σ	g_σ	g_ω	$g_\rho(0)$	$f_\pi(0)$	a_ρ	a_π	ρ_0
PKO1	525.769084	8.833239	10.729933	2.629000	1.000000	0.076760	1.231976	0.151989
PKO2	534.461766	8.920597	10.550553	4.068299	–	0.631605	–	0.151021
PKO3	525.667686	8.895635	10.802690	3.832480	1.000000	0.635336	0.934122	0.153006
	a_σ	b_σ	c_σ	d_σ	a_ω	b_ω	c_ω	d_ω
PKO1	1.384494	1.513190	2.296615	0.380974	1.403347	2.008719	3.046686	0.330770
PKO2	1.375772	2.064391	3.052417	0.330459	1.451420	3.574373	5.478373	0.246668
PKO3	1.244635	1.566659	2.074581	0.400843	1.245714	1.645754	2.177077	0.391293

A. Properties of nuclear matter

1. Bulk properties

Table III shows the bulk quantities of nuclear matter at saturation point (i.e., the saturation density ρ_0 , the binding energy per particle, E_B/A , the incompressibility K , the symmetry energy J , and the scalar mass M_S^*/M). The results calculated by RMF with both the nonlinear self-coupling effective interactions and the density-dependent ones, which have been studied systematically in Ref. [53], are included for comparison. The saturation density and the binding energy per particle given by DDRHF with the PKO series are around 0.152 fm^{-3} and -16.0 MeV, respectively, close to the values provided by RMF. The incompressibility K calculated by DDRHF with PKO1, PKO2, and PKO3 range from 249 to 262 MeV, close to the values given by RMF with a density-dependent effective interaction. In contrast, relatively large values of K (270–360 MeV) are obtained by RMF with the nonlinear self-coupling of mesons, except GL-97 and NL1. For the symmetry energy J , the nonlinear version of RMF also gives relatively large values (36–44 MeV) except for GL-97, whereas the density-dependent version of RMF (except for PKDD) provides comparative values (32–34 MeV)

TABLE III. The saturation density ρ_0 (fm^{-3}), binding energy per particle, E_B/A (MeV), incompressibility K (MeV), asymmetry energy coefficient J (MeV), and the scalar mass M_S^*/M of nuclear matter at the saturation point.

	ρ_0	E_B/A	K	J	M_S^*/M
PKO1	0.1520	-15.996	250.239	34.371	0.5900
PKO2	0.1510	-16.027	249.597	32.492	0.6025
PKO3	0.1530	-16.041	262.469	32.987	0.5862
GL-97	0.1531	-16.316	240.050	32.500	0.7802
NL1	0.1518	-16.426	211.153	43.467	0.5728
NL3	0.1483	-16.249	271.730	37.416	0.5950
NLSH	0.1459	-16.328	354.924	36.100	0.5973
TM1	0.1452	-16.263	281.162	36.892	0.6344
PK1	0.1482	-16.268	282.694	37.642	0.6055
TW99	0.1530	-16.247	240.276	32.767	0.5549
DD-ME1	0.1520	-16.201	244.719	33.065	0.5780
DD-ME2	0.1518	-16.105	250.296	32.271	0.5722
PKDD	0.1496	-16.268	262.192	36.790	0.5712

to DDRHF with PKO1, PKO2, and PKO3. For the scalar mass M_S^* , GL-97 gives the largest value and TW99 gives the smallest. The values given by DDRHF with the PKO series are around 0.60, close to those by RMF with the nonlinear self-couplings of mesons except for GL-97, and systematically smaller values are obtained by RMF with the density-dependent meson-nucleon couplings.

2. Density dependence of the coupling constants

In DDRHF, medium effects are evaluated by the density dependence in the meson-nucleon couplings. To understand the EoS, it is worthwhile to have a look at the density dependence of the coupling constants. Figure 1 shows the coupling constants g_σ , g_ω , g_ρ , and f_π as functions of baryonic density ρ_b , where the results of the DDRHF effective interactions PKO1, PKO2, and PKO3 are given as compared to the RMF ones TW99, DD-ME2, and PKDD. As seen from Fig. 1, all the effective interactions show strong density dependence in the low-density region ($\rho_b < 0.2 \text{ fm}^{-3}$) for both isoscalar (σ and ω) and isovector (ρ and π) meson-nucleon couplings. When density becomes higher, g_σ and g_ω in the left panels become stable, whereas owing to the exponential density dependence, the isovector ones g_ρ and f_π tend to vanish (except g_ρ in PKDD and PKO1), as shown in the right panels. From this aspect, one can understand that the isoscalar mesons provide the dominant contributions in the high-density region. Compared to the RMF effective interactions, PKO1, PKO2, and PKO3 have smaller g_σ and g_ω . This is mainly due to the effects of Fock terms, which lead to the recombination of the ingredients in the nuclear interactions. With the inclusion of Fock terms, the nuclear attractions are shared by the Hartree terms of σ -coupling and the Fock terms of ω -, ρ -, and π -couplings, and the repulsions are contributed by the Hartree terms of ω -coupling and the Fock terms of σ -coupling, whereas in RMF, the attraction and repulsion are provided only by the Hartree terms of the σ - and ω -couplings, respectively.

It is not enough to adjust the isospin properties only within the nuclear saturation region. It is expected that the investigations on the EoS at higher densities and neutron star properties could provide the additional constraint. For the isovector coupling constants in the right panels of Fig. 1, PKO1 and PKDD give slightly weak density dependence in g_ρ because of the fairly small density-dependent parameter a_ρ . In analogy to g_σ and g_ω , the RMF effective interactions

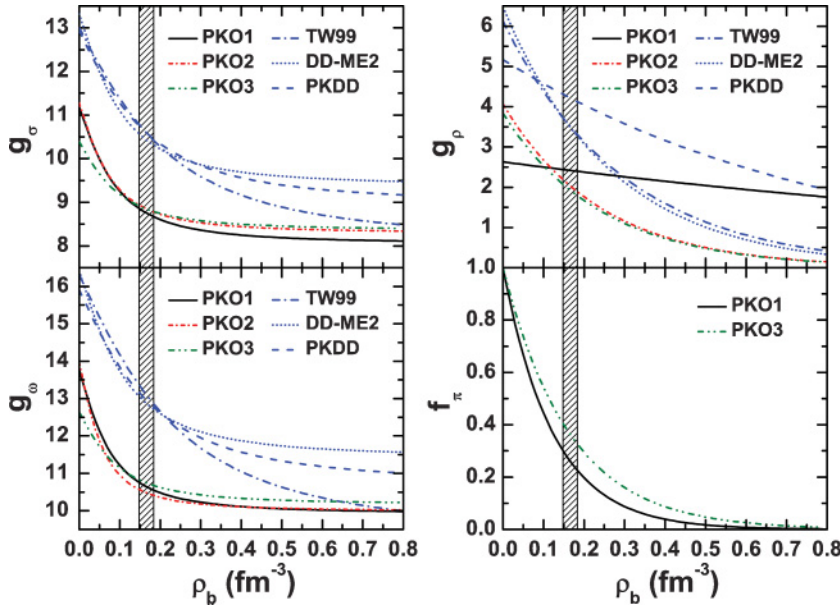


FIG. 1. (Color online) The coupling constants $g_\sigma, g_\omega, g_\rho,$ and f_π as functions of the baryonic density ρ_b (fm^{-3}) for the DDRHF effective interactions PKO1, PKO2, and PKO3 and the RMF ones PKDD, TW99, and DD-ME2. The shadowed area represents the empirical saturation region $\rho_b = 0.166 \pm 0.018 \text{ fm}^{-3}$.

give larger values of g_ρ . This is also due to the exchange contributions. In DDRHF, significant contributions to the isospin part of nuclear interaction are found in exchange terms of isovector mesons as well as isoscalar ones. It is different from the situation in RMF in which the isospin properties are only described by the direct part of ρ -coupling. For the π -meson, the contribution in neutron stars is negligible since f_π tends to vanish at high densities.

3. Equations of state

The equations of state calculated by DDRHF with PKO1, PKO2, and PKO3 are shown in Figs. 2 and 3, respectively, for symmetric nuclear matter and pure neutron matter. The results calculated by RMF with TW99, DD-ME2, and PKDD are also shown for comparison. (See Ref. [53] for the density dependence of the EoS on more RMF effective interactions.) As can be seen from these two figures, identical behaviors

of the EoS are provided by all the effective interactions in the low-density region ($\rho_b < \rho_0$) but in the high-density region pronounced deviations exist among different effective interactions.

For the symmetric nuclear matter in Fig. 2, DDRHF with PKO1, PKO2, and PKO3 provides similar equations of states to RMF with PKDD and DD-ME2, whereas a much softer EoS is obtained by RMF with TW99 when the density becomes high. For the pure neutron matter in Fig. 3, the curves can be classified into three groups according to the behaviors of the EoS in the high-density region. Among all the effective interactions, the DDRHF ones give the hardest equations of state and in the RMF TW99 gives the softest one, whereas DD-ME2 and PKDD provide similar equations of states, which lie between the hardest and softest. Since the DDRHF parametrizations were performed by fitting the properties of finite nuclei and nuclear matter around the saturation point [67], which corresponds to the low-density region, it becomes necessary to test the extrapolation of the effective interactions PKO1, PKO2, and PKO3 to high densities.

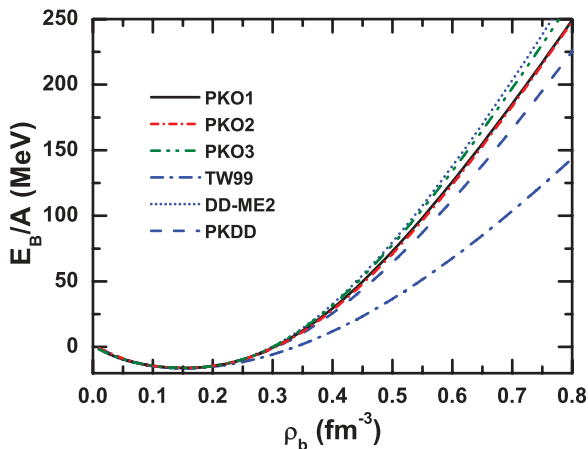


FIG. 2. (Color online) The binding energy per particle, $E_B/A,$ as a function of the baryonic density ρ_b for symmetric nuclear matter. The results are calculated by DDRHF with PKO1, PKO2, and PKO3, in comparison with those by RMF with TW99, DD-ME2, and PKDD.

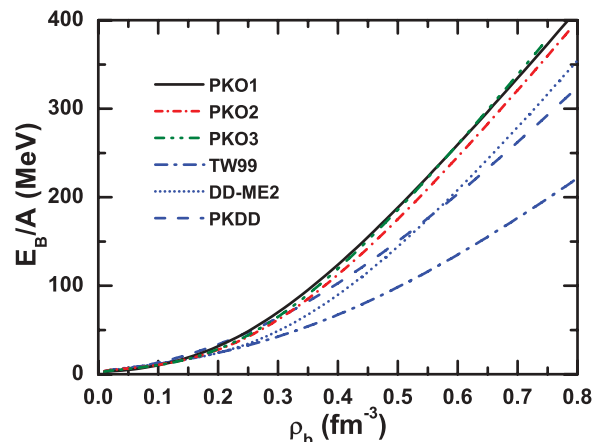


FIG. 3. (Color online) Similar to Fig. 2 but for pure neutron matter.

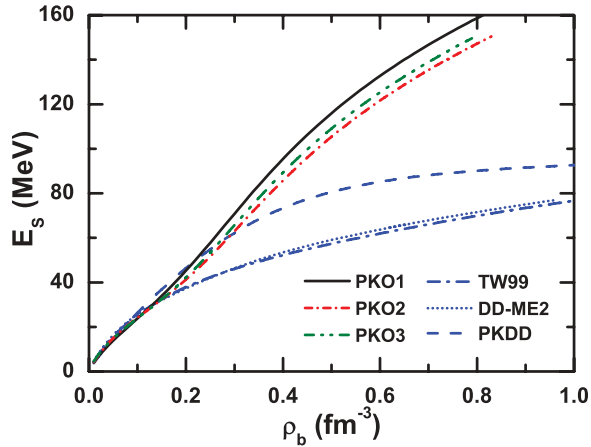


FIG. 4. (Color online) The nuclear symmetry energy E_S (MeV) as a function of the baryon density ρ_b (fm^{-3}). The results are calculated by DDRHF with PKO1, PKO2, and PKO3, in comparison to those by RMF with TW99, DD-ME2, and PKDD.

4. Symmetry energy

The EoS property of isospin asymmetric nuclear matter is still somewhat ambiguous. Different theoretical models predict quite different behaviors of the EoS for pure neutron matter. In most cases, this is due to the effective interactions obtained by fitting the properties of doubly magic nuclei, which have an isospin close to that of symmetric nuclear matter. From this point of view, it becomes necessary to introduce the constraints, either from isospin asymmetric heavy-ion collisions experiments or from the data of nuclei with extreme isospin, into the fitting procedures of the effective interactions.

The symmetry energy is an important quantity for illustrating the property of asymmetric nuclear matter. In general, the energy per particle of asymmetric nuclear matter, $E(\rho_b, \beta)$, can be expanded in a Taylor series with respect to β ,

$$E(\rho_b, \beta) = E_0(\rho_b) + \beta^2 E_S(\rho_b) + \dots, \quad (34)$$

where $\beta = 1 - 2\rho_p/\rho_b$ is the asymmetry parameter depending on the proton fraction. The function $E_0(\rho_b)$ is the binding

energy per particle in symmetric nuclear matter, and the symmetry energy $E_S(\rho_b)$ [$J = E_S(\rho_0)$] is denoted as

$$E_S(\rho_b) = \frac{1}{2} \left. \frac{\partial^2 E(\rho_b, \beta)}{\partial \beta^2} \right|_{\beta=0}. \quad (35)$$

The empirical parabolic law in Eq. (34) is confirmed to be reasonable throughout the range of the asymmetry parameter values, but at high density deviation from such a behavior is found [77].

Figure 4 shows the symmetry energy as a function of the baryon density ρ_b . The results are calculated by DDRHF with PKO1, PKO2, and PKO3, in comparison with those by RMF with TW99, DD-ME2, and PKDD. As shown in Fig. 4, both DDRHF and RMF effective interactions exhibit identical symmetry energy behaviors at low densities ($\rho < \rho_0$), whereas sizable enhancements in the high-density region are obtained by DDRHF with PKO1, PKO2, and PKO3 as compared to the RMF results. Among the RMF calculations, PKDD shows harder behavior than DD-ME2 and TW99, both of which provide identical symmetry energy in the whole density region.

From the energy functional in nuclear matter in Eq. (12), one can obtain the contributions from different channels to the symmetry energy E_S as

$$E_S = E_{S,k} + \sum_{\phi} (E_{S,\phi}^D + E_{S,\phi}^E), \quad (36)$$

where $\phi = \sigma, \omega, \rho,$ and π . In fact, the direct terms of ω -meson coupling have no contribution to the symmetry energy because of the nature of isoscalar-vector coupling. It is also expected that the one-pion exchange has minor effects since nuclear matter is a spin-saturated system. In Fig. 5, the contributions from different channels to the symmetry energy are shown as functions of the baryon density ρ_b . In the left panel are presented the contributions from the kinetic part and isoscalar channels, and only the results calculated by DDRHF with PKO1 are shown in comparison with those by RMF with PKDD and DD-ME2. The contributions from the ρ -meson coupling are shown in the right panel, including the results calculated by DDRHF with PKO1, PKO2, and PKO3 and RMF with PKDD, DD-ME2, and TW99.

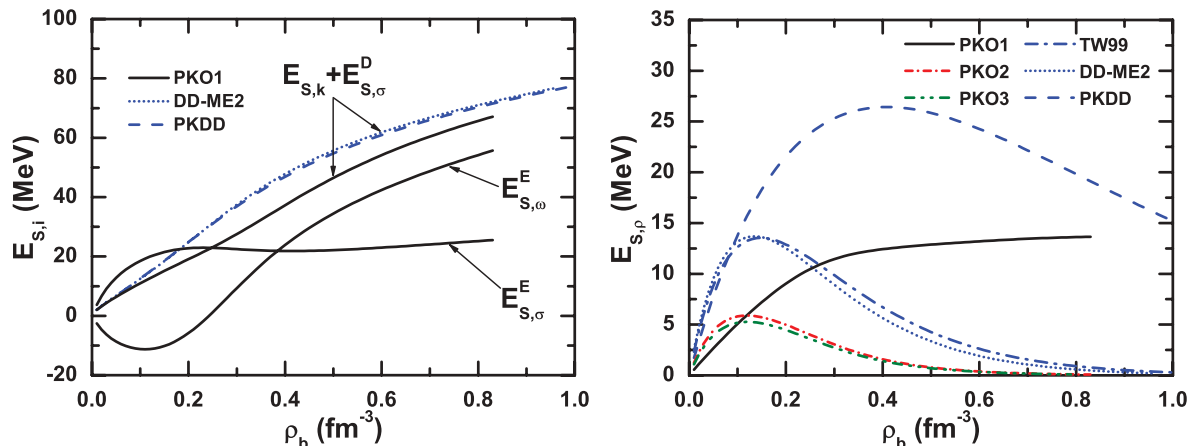


FIG. 5. (Color online) Contributions from different channels to the symmetry energy as a function of the baryon density ρ_b . The left panel gives the contributions from the kinetic energy and isoscalar channels; the ones from ρ mesons are shown in the right panel. See text for details.

Within RMF, one can find that the kinetic part and the direct terms of σ coupling (i.e., $E_{S,k}$ and $E_{S,\sigma}^D$) provide the dominant contributions to the symmetry energy. As shown in the left panel of Fig. 5, PKDD and DD-ME2 give identical values of $E_{S,k} + E_{S,\sigma}^D$, and the deviation between them appearing in Fig. 4 is mainly due to their contributions from the ρ -coupling, as seen from the right panel of Fig. 5. In the left panel of Fig. 5, the values of $E_{S,k} + E_{S,\sigma}^D$ given by the DDRHF calculations are found to be smaller than those of RMF with PKDD and DD-ME2. It is also seen that the Fock terms of σ - and ω -couplings exhibit significant contributions to the symmetry energy, which well fits with the stronger density dependence predicted by DDRHF than by RMF in the high-density region (see Fig. 4). As seen from the left panel of Fig. 5, the values of $E_{S,\sigma}^E$ increase rapidly in the low-density region and tend to be stable about 20–25 MeV at high density. However, the exchange terms of ω -coupling provide negative contributions to the symmetry energy at low density and reach a minimum of about -11 MeV at $\rho_b = 0.1 \text{ fm}^{-3}$. After that the values of $E_{S,\omega}^E$ increase and become comparable to the values of $E_{S,k} + E_{S,\sigma}^D$ at several times the saturation density.

In the right panel of Fig. 5, the contributions of ρ -coupling (i.e., $E_{S,\rho} = E_{S,\rho}^D + E_{S,\rho}^E$) are found to be important for the symmetry energy in the low-density region. When density gets high, the values of $E_{S,\rho}$ given by all the effective interactions except PKO1 and PKDD tend to zero owing to their strong exponential density dependence in ρ -nucleon coupling. Because of its much smaller value of a_ρ , PKO1 presents larger contributions than PKO2 and PKO3 and contributes a value of about 10–15 MeV in the high-density region. For the same reason, PKDD also provides larger values of $E_{S,\rho}$ than the other two RMF effective interactions, reaching a maximum of about 26 MeV at $\rho_b \simeq 0.41 \text{ fm}^{-3}$, then declining slowly. Comparing the values of $E_{S,\rho}$ given by PKO2 and PKO3 to those by DD-ME2 and TW99, one sees that the contribution of ρ -coupling $E_{S,\rho}$ is depressed systematically in DDRHF. Such depressions also exist between the results of PKO1 and PKDD, which are of similar density dependence in ρ -nucleon coupling. This could be understood from the fact that smaller

values of g_ρ are obtained with the inclusion of Fock terms, as seen in Fig. 1. In fact, not only the ρ meson but all the mesons take part in the isospin properties and are in charge of producing the symmetry energy via the Fock channel.

In conclusion, one finds that the Fock terms play an important role in determining the density-dependent behavior of the symmetry energy. It is then expected that the important constraints on the symmetry energy and the EoS of asymmetric nuclear matter could be obtained from the study of neutron stars.

B. Properties of neutron stars

In this work, the static and β -equilibrium assumptions are imposed for the description of neutron stars. As density increases, the high-momentum neutrons will β decay into protons and electrons (i.e., $n \leftrightarrow p + e^- + \bar{\nu}_e$) until the chemical potentials satisfy the equilibrium $\mu_p = \mu_n - \mu_e$. When the chemical potential of electron μ_e reaches the limit of the muon mass, the lepton μ^- will appear. The reaction $e^- \leftrightarrow \mu^- + \bar{\nu}_\mu + \nu_e$ implies equilibrium between the e^- and μ^- chemical potentials (i.e., $\mu_e = \mu_\mu$).

1. Density distribution

To keep the equilibrium among the particle chemical potentials, protons, electrons, and muons will appear with increasing density in neutron stars. Figure 6 shows the neutron, proton, electron, and muon densities in neutron stars as functions of the baryon density. The results are calculated by DDRHF with PKO1, PKO2, and PKO3, in comparison to those by RMF with TW99, DD-ME2, and PKDD. The density distributions of various components in RMF with both the nonlinear self-coupling effective interactions and the density-dependent ones have been studied systematically in Ref. [53]. As seen from Fig. 6, the thresholds of μ^- occurrence predicted by different effective interactions are very close to each other, roughly around $\rho_b = 0.12 \text{ fm}^{-3}$. It is shown that

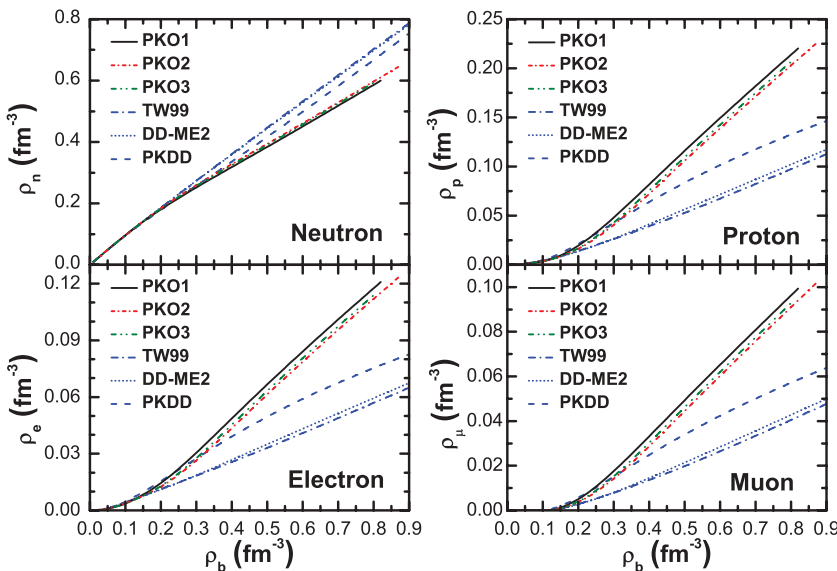


FIG. 6. (Color online) The neutron (upper left panel), proton (upper right panel), electron (lower left panel), and muon (lower right panel) densities in neutron star matter as functions of the baryon density ρ_b (fm^{-3}). The results are calculated by DDRHF with PKO1, PKO2, and PKO3, in comparison to those by RMF with TW99, DD-ME2, and PKDD.

all the densities keep increasing monotonically with respect to the baryonic density ρ_b . Similar to the situation in the EoS of nuclear matter, different effective interactions present identical trends at low densities ($\rho_b < \rho_0$), but remarkable deviations exist in the high-density region between the DDRHF and RMF predictions. As seen from Fig. 6, the results given by different effective interactions can be classified into three groups: the DDRHF ones, PKDD, and the RMF ones DD-ME2 and TW99. For the proton, electron, and muon densities, the strongest density dependence is exhibited by DDRHF with PKO1, PKO2, and PKO3, whereas the softest behaviors are provided by RMF with DD-ME2 and TW99. In contrast, the softest behavior on neutron density is predicted by the DDRHF effective interactions, whereas TW99 and DD-ME2 exhibit the hardest. This kind of reversion can be well understood from the relations in Eq. (29) among the densities.

It is known that the density fractions of each component in neutron stars are rather sensitive to the symmetry energy, as illustrated by associating Fig. 6 with Fig. 4. Owing to the strong effects from the exchange terms of ω -coupling in the high-density region (see Fig. 5), DDRHF with PKO1, PKO2, and PKO3 shows stronger density dependence on the symmetry energy and thus harder proton, electron, and muon density distributions, as compared to the RMF calculations. The deviations between different effective interactions within one theoretical model (e.g., between PKDD and DD-ME2) are mainly due to the ρ -coupling, as shown in the right panel of Fig. 5, where the ρ -meson coupling of PKDD shows larger contributions to the symmetry energy. In conclusion, the harder the symmetry energy behavior at high densities is, the more difficult it becomes for the system to become asymmetric and the easier it is for neutrons to decay into protons and electrons, which leads to smaller neutron abundance and larger proton, electron, and muon abundances in neutron stars.

2. Proton fraction and direct Urca constraint

From the density distributions in Fig. 6, one can extract the proton fraction $x = \rho_p/(\rho_p + \rho_n)$ within the range of density of neutron stars. Figure 7 shows the proton fraction x as a function of baryonic density ρ_b , where the results calculated by DDRHF with the PKO series are presented in comparison to those by RMF with TW99, DD-ME2, and PKDD. Because of the stiff behavior of the symmetry energy (see Fig. 4), a stronger density dependence of the proton fraction x in neutron star matter is obtained by DDRHF than RMF, as shown in Fig. 7.

The cooling mechanism of neutron stars, which is sensitive to the proton fraction, could bring significant information on asymmetric nuclear equations of state. Direct Urca (DU) processes $n \rightarrow p + e^- + \bar{\nu}_e$ and $p + e^- \rightarrow n + \nu_e$ lead the star to cool rapidly by emitting thermal neutrinos. The threshold of the proton fraction x^{DU} for the DU process occurring can be easily found as $11.1\% \leq x^{\text{DU}} \leq 14.8\%$ from momentum conservation and charge neutrality [21,24]. As seen from Fig. 7, the critical density ρ^{DU} for the DU process occurring depends on the EoS. Once the critical density ρ^{DU} is reached in the center of a neutron star for a given EoS, the star

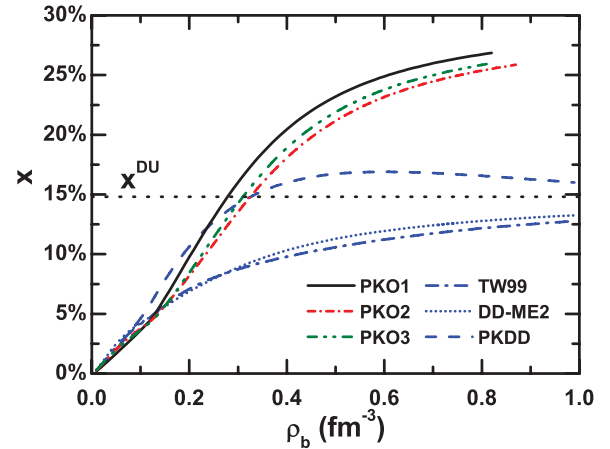


FIG. 7. (Color online) Proton fractions $x = \rho_p/(\rho_p + \rho_n)$ in neutron star matter for different DDRHF and DDRMF effective interactions. The dotted line labeled with x^{DU} is the threshold for the direct Urca process to occur. Here $x^{\text{DU}} = 14.8\%$ is taken by assuming muons in the massless limit.

will be efficiently cooled via the DU process. It is found that the values of x^{DU} given by DDRHF calculations correspond to fairly low critical densities whereas the results calculated by RMF with TW99 and DD-ME2 do not support the DU process occurring at all. The DU critical star masses M^{DU} and corresponding central densities $\rho^{\text{DU}}(0)$ are marked in Fig. 9 by filled squares.

According to the analysis in Refs. [22–24], if the DU process is taken as a possible mechanism for neutron star cooling, an acceptable EoS would not allow it to occur in neutron stars with masses below $1.5M_\odot$; otherwise it will be in disagreement with modern observational soft X-ray data in the temperature-age diagram. As a weaker constraint, the limit $M^{\text{DU}} > 1.35M_\odot$ could be applied. From the mass limit M^{DU} are then obtained the constraint over the EoS that the density dependence of the symmetry energy should not be too strong, nor probably too weak, either. Table IV gives the critical neutron star mass M^{DU} and central densities $\rho^{\text{DU}}(0)$ from the DDRHF and RMF calculations, which support the occurrence of the DU cooling process in stars.

As seen from Table IV, rather small mass limits M^{DU} are obtained by RMF with the nonlinear self-coupling of mesons whereas the DDRHF calculations with PKO2 and PKO3 provide larger values of M^{DU} , which are very close to the aforementioned limit of $1.5M_\odot$ and satisfy the weak constraint that $M^{\text{DU}} > 1.35M_\odot$. For the calculation with PKO1, the DU cooling process will occur at the fairly low mass $1.20M_\odot$ and central density $\rho^{\text{DU}} \simeq 0.28 \text{ fm}^{-3}$, which can be interpreted by the contributions of the ρ -meson coupling to the symmetry energy. For $E_{S,\rho}$ in the right panel of Fig. 5, the ρ -meson coupling in PKO1 still has remarkable effects in the high-density region owing to the weak density dependence of g_ρ (see Fig. 1). For the same reason, the RMF calculation with PKDD also supports the DU cooling process occurring at a low mass limit of $1.26M_\odot$. In contrast, as seen in Fig. 7, the occurrence of the DU cooling process is not supported at all by the RMF calculations with TW99 and DD-ME2 as well

TABLE IV. Critical neutron star masses M^{DU} and central densities $\rho^{\text{DU}}(0)$ for the occurrence of the DU cooling process and the criterion of the DU constraint given by both DDRHF and RMF effective interactions. Fulfillment (violation) of a constraint is indicated with + (−).

	PKO1	PKO2	PKO3	GL-97	NL1	NL3	NLSH	TM1	PK1	PKDD
$M^{\text{DU}} [M_{\odot}]$	1.20	1.45	1.43	1.10	0.75	1.01	1.20	0.96	0.94	1.26
$\rho^{\text{DU}}(0) [\text{fm}^{-3}]$	0.28	0.33	0.31	0.33	0.20	0.23	0.24	0.24	0.23	0.33
$M^{\text{DU}} \geq 1.5M_{\odot}$	−	−	−	−	−	−	−	−	−	−
$M^{\text{DU}} \geq 1.35M_{\odot}$	−	+	+	−	−	−	−	−	−	−

as DD-ME1. It is expected that the occurrence of the DU process could be introduced as a possible constraint in future parametrizations of both DDRHF and RMF, for example, for ρ -meson coupling [$g_{\rho}(0)$ and a_{ρ}].

3. Pressure and maximum mass of neutron stars

Figure 8 shows the pressures of neutron star matter calculated by DDRHF effective interactions as functions of the baryonic density ρ_b . The RMF results with GL-97, NL3, TW99 in Ref. [53] and also PK1, DD-ME2, and PKDD have been included for comparison. It is found that PKO1, PKO2, and PKO3 provide identical behaviors over the density dependence of the pressure; these are also close to the behaviors predicted by RMF with PKDD and DD-ME2. Among all the DDRHF and RMF calculations, NL3 provides the strongest density dependence and the softest are presented by GL-97. The behaviors given by PK1 and TW99 lie between the results of DDRHF with the PKO series and RMF with GL-97.

The variation of the pressure with respect to density is essential to understand the structure of neutron stars. A stronger density dependence of the pressure at high densities would lead to a larger value of the maximum mass for neutron stars that can be sustained against collapse. In Fig. 9, the neutron star masses calculated by DDRHF with PKO1, PKO2, and PKO3 are shown as functions of the central density $\rho(0)$.

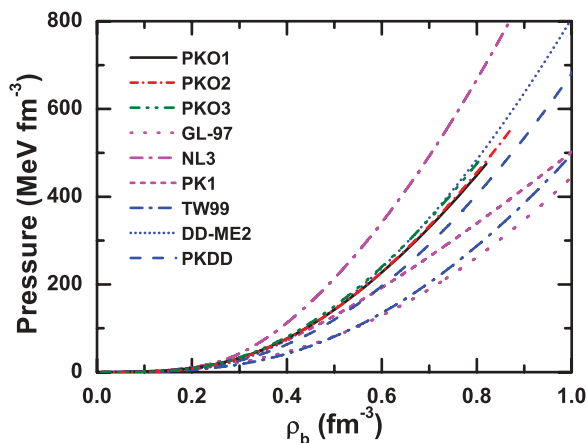


FIG. 8. (Color online) The pressure of neutron star matter as a function of the baryonic density ρ_b (fm^{-3}). The results are calculated by DDRHF with PKO1, PKO2, and PKO3, in comparison to those by RMF with GL-97, NL3, PK1, TW99, DD-ME2, and PKDD.

For comparison, also shown are the results calculated by RMF with GL-97, NL3, PK1, TW99, DD-ME2, and PKDD, and one could refer to Ref. [53] for more studies with a variety of RMF effective interactions. From Fig. 9, it is found that the maximum masses given by the DDRHF calculations lie between $2.4M_{\odot}$ and $2.5M_{\odot}$ with the central densities around 0.80 fm^{-3} , which are close to the prediction of RMF with DD-ME2. Notice that these values are also compatible to the observational constraint ($M = 2.08 \pm 0.19M_{\odot}$) from PSR B1516 + 02B [14]. Table V shows the maximum mass limits M_{max} and the corresponding central densities $\rho_{\text{max}}(0)$ extracted from Fig. 9. Consistent with the description of the pressure, the nonlinear RMF effective interaction NL3 exhibits a rather large value of the maximum mass $M_{\text{max}} = 2.78M_{\odot}$ with small central density $\rho_{\text{max}}(0) = 0.67 \text{ fm}^{-3}$, whereas the smallest M_{max} and the largest $\rho_{\text{max}}(0)$ are obtained by RMF with GL-97 and TW99, which gives the softest behaviors of the pressure (see Fig. 8). As seen from Table V, the values of M_{max} given by all the effective interactions are in appropriate agreement with the constraint on the maximum mass from PSR B1516 + 02B.

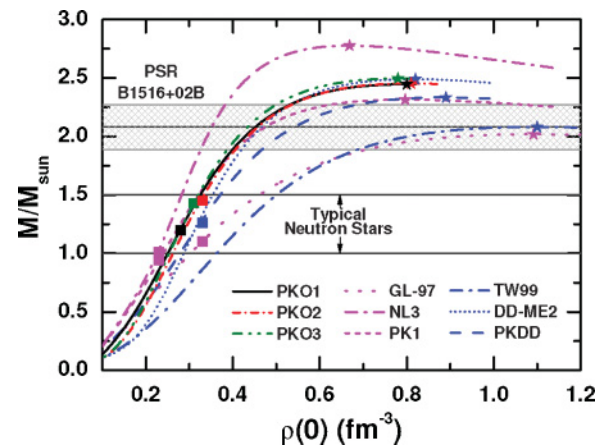


FIG. 9. (Color online) Neutron star mass as a function of the central density for different DDRHF and RMF effective interactions. Filled stars denote the maximum mass configurations; filled squares mark the critical mass M^{DU} and central density values $\rho^{\text{DU}}(0)$ where the DU cooling process becomes possible. The light gray horizontal bands around $2.08M_{\odot}$ denote the 1σ confidence level for the mass measurement of PSR B1516+02B [14]. The mass region of typical neutron stars is between $1.0M_{\odot}$ and $1.5M_{\odot}$.

TABLE V. Maximum mass limits M_{\max} (M_{\odot}), the corresponding central densities $\rho_{\max}(0)$ (fm^{-3}), and radii $R(M_{\max})$ (km) for neutron stars calculated by DDRHF and RMF effective interactions. The radii (km) for $1.4M_{\odot}$ neutron stars are shown as well.

	PKO1	PKO2	PKO3	GL-97	NL1	NL3	NLSH	TM1	PK1	TW99	DD-ME1	DD-ME2	PKDD
M_{\max}	2.45	2.45	2.49	2.02	2.81	2.78	2.80	2.18	2.32	2.08	2.45	2.49	2.33
$\rho_{\max}(0)$	0.80	0.81	0.78	1.09	0.66	0.67	0.65	0.85	0.80	1.10	0.84	0.82	0.89
$R(M_{\max})$	12.4	12.3	12.5	10.9	13.4	13.3	13.5	12.4	12.7	10.7	11.9	12.1	11.8
$R(1.4M_{\odot})$	14.1	13.8	13.9	13.3	14.7	14.7	14.9	14.4	14.5	12.4	13.2	13.3	13.7

4. Mass-radius relation and observational constraint

Recent astronomic observations also provide constraints on the mass-radius relation of neutron stars. In this paper, four typical observations are adopted to test the theoretical calculations:

- (i) the large radiation radius $R_{\infty} = 16.8$ km ($R_{\infty} = R/\sqrt{1 - 2GM/Rc^2}$) from the isolated neutron star RX J1856 [16],
- (ii) the redshift $z \simeq 0.345$, the mass $M \geq 2.10 \pm 0.28M_{\odot}$, and the radius $R \geq 13.8 \pm 1.8$ km constraints in LMXB EXO 0748-676 [18,19],
- (iii) $M \lesssim 1.8M_{\odot}$ and $R \lesssim 15\text{km}$ constraints from the highest frequency of QPOs (1330 Hz) ever observed in 4U 0614 + 09 [20], and
- (iv) several neutron stars in LMXBs with gravitational masses between $1.9M_{\odot}$ and possibly $2.1M_{\odot}$ from the QPO data analysis in LMXB 4U 1636-536 [13].

Figure 10 shows the mass-radius relations of neutron stars calculated by DDRHF with PKO1, PKO2, and PKO3 and RMF with GL-97, NL3, PK1, TW99, DD-ME2, and PKDD. The results with more RMF effective interactions have been investigated in Ref. [53]. For comparison, the selected observational constraints are marked with different colors and grids, as shown in Fig. 10. The causality limit that $\sqrt{\partial p/\partial \varepsilon} \leq 1$ results in $R > 2.9 GM/c^2$ [78,79] and the corresponding region in Fig. 10 is marked in black. Compared to all the observational limits, it is found that better agreements are obtained by the DDRHF effective interactions than the RMF ones. Among the RMF results, GL-97 is excluded by the limits from RX J1856, and TW99 is excluded by the limits from both RX J1856 and EXO 0748-676, but NL3 could not fulfill the constraint from 4U 0614 + 09. If the upper mass limit of $2.1M_{\odot}$ is taken in 4U 1636-536, neither GL-97 and TW99 are satisfied. The detailed criteria of the M - R constraints

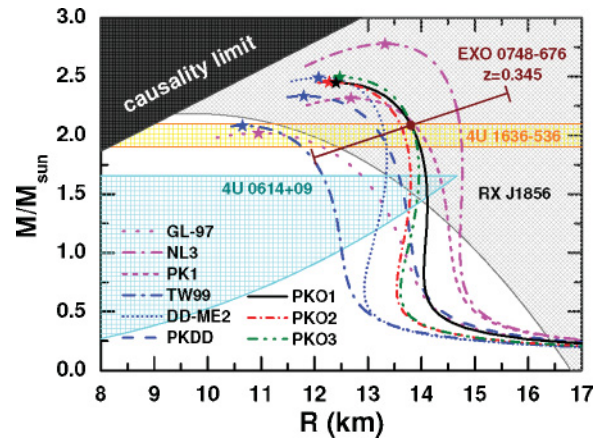


FIG. 10. (Color online) Mass-radius relations of neutron stars provided by the DDRHF and RMF calculations and the corresponding maximum masses (marked by filled star symbols). For comparison are also shown the four separate observational constraints from RX J1856 (gray grided region), 4U 0614 + 09 (cyan grided area), 4U 1636-536 (yellow grided area), and EXO 0748-676 (error bar for 1σ error). The black region is excluded by causality that $R > 2.9 GM/c^2$ [78,79]. See the text for details.

are presented in Table VI. It is shown that the predictions given by DDRHF with the PKO series and RMF with PK1, TM1, DD-ME1, DD-ME2, and PKDD fulfill all the M - R constraints.

In Refs. [58,59], the radius of neutron stars with a mass of $1.4M_{\odot}$ was found to be correlated with the neutron skin thickness of ^{208}Pb as well as the symmetry energy. If the observation can limit the radius of neutron stars to a narrow range, a strong constraint can be imposed on the symmetry energy. However, if the neutron skin thickness of ^{208}Pb or the symmetry energy could be precisely determined from terrestrial experiments, this would be helpful for understanding

TABLE VI. The criteria of the M - R constraints: (1) the isolated neutron star RX J1856, (2) EXO 0748-676, (3) the low-mass X-ray binary 4U 0614 + 09, (4-u) 4U 1636-536 with its upper mass limits, and (4-l) 4U 1636-536 with its lower mass limits. Fulfillment (violation) of a constraint is indicated with + (−) and the marginal cover is marked with δ . See the text for details.

	PKO1	PKO2	PKO3	GL-97	NL1	NL3	NLSH	TM1	PK1	TW99	DD-ME1	DD-ME2	PKDD
1	+	+	+	−	+	+	+	+	+	−	+	+	+
2	+	+	+	+	+	+	+	+	+	Δ	+	+	+
3	+	+	+	+	Δ	Δ	−	+	+	+	+	+	+
4-u	+	+	+	−	+	+	+	+	+	Δ	+	+	+
4-l	+	+	+	+	+	+	+	+	+	+	+	+	+

neutron star structure and rule out some equations of state for neutron star matter. As seen in Fig. 10 and Table V, although several equations of state provide similar maximum masses, they still show some discrepancy for the radius of neutron stars with a mass of $1.4M_{\odot}$. In Table V, the DDRHF interactions predict this radius in a range from 13.8 to 14.1 km, whereas the nonlinear RMF interaction NLSH gives the largest value (14.9 km) and the density-dependent RMF interaction TW99 gives the smallest (12.4 km). All the calculated results except TW99 are coincident with the X-ray spectral analysis of the quiescent LMXB X7 in the globular cluster 47 Tuc, which requires a rather large radius of $14.5^{+1.8}_{-1.6}$ km for $1.4M_{\odot}$ compact stars [17].

IV. SUMMARY

In this paper, the equations of state for symmetric nuclear matter, pure neutron matter, and β -stable neutron star matter have been studied within the density-dependent relativistic Hartree-Fock theory with PKO1, PKO2, and PKO3. Substantial effects from the Fock terms are found in describing the asymmetric nuclear matter at high densities. Because of the contributions from the Fock terms of σ - and ω -couplings, a stronger density dependence on the symmetry energy is obtained from DDRHF at high densities, as compared to the RMF calculations with the density-dependent meson-nucleon couplings. Because of the weak density dependence of g_{ρ} in PKO1, which induces remarkable contributions from the ρ -meson coupling to the symmetry energy, PKO1 shows a stronger density dependence on the symmetry energy than either PKO2 or PKO3. With the obtained equations of state for β -stable nuclear matter, the properties of neutron stars are investigated within the DDRHF theory for the first time and the recent observational constraints of compact stars are also introduced to test the applicability of the DDRHF models.

The extra enhancement from the σ - and ω -exchange terms on the symmetry energy cause large proton fractions in neutron stars to be predicted by the DDRHF calculations, which affects essentially the cooling process of the star. For the DU process occurring, DDRHF with PKO2 and PKO3 gives a critical neutron star mass of $\sim 1.45M_{\odot}$, which is close to the limit of $1.5M_{\odot}$ from modern soft X-ray data analysis in the temperature-age diagram and fulfills the weaker constraint of

$1.35M_{\odot}$. In contrast, fairly small mass limits are presented by the calculations of DDRHF with PKO1, RMF with the nonlinear self-couplings of mesons, and RMF with PKDD, mainly because of their stronger ρ -coupling contributions to the symmetry energy at high densities. In contrast to these two cases, the RMF calculations with TW99, DD-ME1, and DD-ME2 do not support the occurrence of the DU process in neutron stars at all. In addition, the radii of $1.4M_{\odot}$ neutron stars are correlated with the symmetry energy as well. In general, a stronger density dependence on the symmetry energy leads to a larger radius for a $1.4M_{\odot}$ neutron star. The radii given by the DDRHF calculations lie between 13.8 and 14.1 km, larger than the RMF calculations with the density-dependent meson-nucleon couplings and smaller than the ones with the nonlinear self-couplings of mesons except GL-97.

The maximum masses and central densities of neutron stars are tightly correlated with the behavior of the pressure with respect to the density. Because of the similar density-dependent behaviors of the pressure, identical maximum masses ($\sim 2.5M_{\odot}$) of neutron stars are found in the calculations of DDRHF and RMF with DD-ME1 and DD-ME2, as well as central densities around 0.80 fm^{-3} . The results are in reasonable agreement with the recently reported high pulsar mass of $(2.08 \pm 0.19)M_{\odot}$ from PSR B1516 + 02B. The mass-radius relations of neutron stars determined by the DDRHF calculations are also consistent with the observational data from thermal radiation measurement in the isolated neutron star RX J1856, QPO frequency limits in LMXBs 4U 0614 + 09 and 4U 1636-536, and the redshift limit determined in LMXB EXO 0748-676, which are only partially satisfied in the RMF calculations with GL-97, NL1, NL3, NLSH, and TW99.

ACKNOWLEDGMENTS

The authors thank H.-J. Schulze for stimulating discussions and D. Blaschke for communications about the observational constraints of compact stars. This work is partly supported by the Major State Basic Research Development Program (2007CB815000), the National Natural Science Foundation of China (10435010, 10775004, and 10221003), and the Asia-Europe Link Program in Nuclear Physics and Astrophysics (CN/ASIA-LINK/008 094-791).

-
- [1] F. Weber, *Pulsars as Astrophysical Laboratories for Nuclear and Particle Physics* (Taylor & Francis, Bristol, 1999).
 - [2] S. L. Shapiro and S. A. Teukolsky, *Black Holes, White Dwarfs, and Neutron Stars: The Physics of Compact Objects* (Wiley, New York, 1983).
 - [3] F. Weber, R. Negreiros, P. Rosenfield, and M. Stejner, *Prog. Part. Nucl. Phys.* **59**, 94 (2007).
 - [4] P. Danielewicz, R. Lacey, and W. G. Lynch, *Science* **298**, 1592 (2002).
 - [5] C. Fuchs, *Prog. Part. Nucl. Phys.* **56**, 1 (2006).
 - [6] B.-A. Li, L.-W. Chen, and C. M. Ko, *Phys. Rep.* **464**, 113 (2008).
 - [7] L. D. Landau, *Phys. Z. Sowjetunion* **1**, 285 (1932).
 - [8] W. Baade and F. Zwicky, *Proc. Natl. Acad. Sci. USA.* **20**, 255 (1934).
 - [9] A. Hewish, S. J. Bell, J. D. H. Pilkington, P. F. Scott, and R. A. Collins, *Nature (London)* **217**, 709 (1968).
 - [10] F. Pacini, *Nature (London)* **216**, 567 (1967).
 - [11] J. M. Lattimer and M. Prakash, *Science* **304**, 536 (2004).
 - [12] J. M. Lattimer and M. Prakash, *Phys. Rep.* **442**, 109 (2007).
 - [13] D. Barret, J.-F. Olive, and M. C. Miller, *Mon. Not. R. Astron. Soc.* **361**, 855 (2005).
 - [14] P. C. C. Freire, A. Wolszczan, M. van den Berg, and J. W. T. Hessels, *Astrophys. J.* **679**, 1433 (2008).
 - [15] P. C. C. Freire, S. M. Ransom, S. Bégin, I. H. Stairs, J. W. T. Hessels, L. H. Frey, and F. Camilo, *Astrophys. J.* **675**, 670 (2008).
 - [16] J. E. Trümper, V. Burwitz, F. Haberl, and V. E. Zavlin, *Nucl. Phys. Proc. Suppl.* **132**, 560 (2004).

- [17] C. O. Heinke, G. B. Rybicki, R. Narayan, and J. E. Grindlay, *Astrophys. J.* **644**, 1090 (2006).
- [18] J. Cottam, F. Paerels, and M. Mendez, *Nature (London)* **420**, 51 (2002).
- [19] F. Özel, *Nature (London)* **441**, 1115 (2006).
- [20] M. C. Miller, *AIP Conf. Proc.* **714**, 365 (2004).
- [21] J. M. Lattimer, C. J. Pethick, M. Prakash, and P. Haensel, *Phys. Rev. Lett.* **66**, 2701 (1991).
- [22] D. Blaschke, H. Grigorian, and D. N. Voskresensky, *Astron. Astrophys.* **424**, 979 (2004).
- [23] S. Popov, H. Grigorian, R. Turolla, and D. Blaschke, *Astron. Astrophys.* **448**, 327 (2006).
- [24] T. Klähn *et al.*, *Phys. Rev. C* **74**, 035802 (2006).
- [25] L. D. Miller and A. E. S. Green, *Phys. Rev. C* **5**, 241 (1972).
- [26] J. D. Walecka, *Ann. Phys. (NY)* **83**, 491 (1974).
- [27] B. D. Serot and J. D. Walecka, *Adv. Nucl. Phys.* **16**, 1 (1986).
- [28] P. G. Reinhard, *Rep. Prog. Phys.* **52**, 439 (1989).
- [29] P. Ring, *Prog. Part. Nucl. Phys.* **37**, 193 (1996).
- [30] B. D. Serot and J. D. Walecka, *Int. J. Mod. Phys. E* **6**, 515 (1997).
- [31] M. Bender, P.-H. Heenen, and P.-G. Reinhard, *Rev. Mod. Phys.* **75**, 121 (2003).
- [32] J. Meng, *Nucl. Phys.* **A635**, 3 (1998).
- [33] J. Meng and P. Ring, *Phys. Rev. Lett.* **77**, 3963 (1996).
- [34] J. Meng and P. Ring, *Phys. Rev. Lett.* **80**, 460 (1998).
- [35] J. Meng, I. Tanihata, and S. Yamaji, *Phys. Lett.* **B419**, 1 (1998).
- [36] J. Meng, H. Toki, S. G. Zhou, S. Q. Zhang, W. H. Long, and L. S. Geng, *Prog. Part. Nucl. Phys.* **57**, 470 (2006).
- [37] G. A. Lalazissis, J. König, and P. Ring, *Phys. Rev. C* **55**, 540 (1997).
- [38] S. Typel and H. H. Wolter, *Nucl. Phys.* **A656**, 331 (1999).
- [39] W. Long, J. Meng, N. Van Giai, and S.-G. Zhou, *Phys. Rev. C* **69**, 034319 (2004).
- [40] T. Nikšić, D. Vretenar, P. Finelli, and P. Ring, *Phys. Rev. C* **66**, 024306 (2002).
- [41] G. A. Lalazissis, T. Nikšić, D. Vretenar, and P. Ring, *Phys. Rev. C* **71**, 024312 (2005).
- [42] J. R. Oppenheimer and G. M. Volkoff, *Phys. Rev.* **55**, 374 (1939).
- [43] R. C. Tolman, *Phys. Rev.* **55**, 364 (1939).
- [44] N. K. Glendenning, *Compact Stars, Nuclear Physics, Particle Physics and General Relativity*, 2nd ed. (Springer-Verlag, New York, 2000).
- [45] R. Brockmann and H. Toki, *Phys. Rev. Lett.* **68**, 3408 (1992).
- [46] H. Lenske and C. Fuchs, *Phys. Lett.* **B345**, 355 (1995).
- [47] C. Fuchs, H. Lenske, and H. H. Wolter, *Phys. Rev. C* **52**, 3043 (1995).
- [48] J. Boguta and A. Bodmer, *Nucl. Phys.* **A292**, 413 (1977).
- [49] Y. Sugahara and H. Toki, *Nucl. Phys.* **A579**, 557 (1994).
- [50] B. D. Serot, *Phys. Lett.* **B86**, 146 (1979).
- [51] K. Sumiyoshi, H. Kuwabara, and H. Toki, *Nucl. Phys.* **A581**, 725 (1995).
- [52] F. Hofmann, C. M. Keil, and H. Lenske, *Phys. Rev. C* **64**, 025804 (2001).
- [53] S. F. Ban, J. Li, S. Q. Zhang, H. Y. Jia, J. P. Sang, and J. Meng, *Phys. Rev. C* **69**, 045805 (2004).
- [54] N. K. Glendenning, *Phys. Lett.* **B114**, 392 (1982).
- [55] N. K. Glendenning, *Astrophys. J.* **293**, 470 (1985).
- [56] R. Knorren, M. Prakash, and P. J. Ellis, *Phys. Rev. C* **52**, 3470 (1995).
- [57] J. Schaffner and I. N. Mishustin, *Phys. Rev. C* **53**, 1416 (1996).
- [58] C. J. Horowitz and J. Piekarewicz, *Phys. Rev. Lett.* **86**, 5647 (2001).
- [59] C. J. Horowitz and J. Piekarewicz, *Phys. Rev. C* **64**, 062802(R) (2001).
- [60] B. A. Brown, G. Shen, G. C. Hillhouse, J. Meng, and A. Trzcińska, *Phys. Rev. C* **76**, 034305 (2007).
- [61] C. J. Horowitz and J. Piekarewicz, *Phys. Rev. C* **66**, 055803 (2002).
- [62] H. Huber, F. Weber, and M. K. Weigel, *Phys. Rev. C* **50**, R1287 (1994).
- [63] L. Engvik, M. Hjorth-Jensen, E. Osnes, G. Bao, and E. Østgaard, *Phys. Rev. Lett.* **73**, 2650 (1994).
- [64] P. G. Krastev and F. Sammarruca, *Phys. Rev. C* **74**, 025808 (2006).
- [65] M. Baldo, I. Bombaci, and G. F. Burgio, *Astron. Astrophys.* **328**, 274 (1997).
- [66] X. R. Zhou, G. F. Burgio, U. Lombardo, H.-J. Schulze, and W. Zuo, *Phys. Rev. C* **69**, 018801 (2004).
- [67] W. H. Long, N. Van Giai, and J. Meng, *Phys. Lett.* **B640**, 150 (2006).
- [68] W. H. Long, H. Sagawa, N. Van Giai, and J. Meng, *Phys. Rev. C* **76**, 034314 (2007).
- [69] W. H. Long, H. Sagawa, J. Meng, and N. Van Giai, *Europhys. Lett.* **82**, 12001 (2008).
- [70] H. Liang, N. Van Giai, and J. Meng, *Phys. Rev. Lett.* **101**, 122502 (2008).
- [71] W. H. Long, H. Sagawa, J. Meng, and N. Van Giai, *Phys. Lett.* **B639**, 242 (2006).
- [72] A. Bouyssy, J. F. Mathiot, N. Van Giai, and S. Marcos, *Phys. Rev. C* **36**, 380 (1987).
- [73] G. Baym, C. J. Pethick, and P. Sutherland, *Astrophys. J.* **170**, 299 (1971).
- [74] G. Baym, H. A. Bethe, and C. J. Pethick, *Nucl. Phys.* **A175**, 225 (1971).
- [75] P. G. Reinhard, M. Rufa, J. Maruhn, W. Greiner, and J. Friedrich, *Z. Phys. A* **323**, 13 (1986).
- [76] M. M. Sharma, M. A. Nagarajan, and P. Ring, *Phys. Lett.* **B312**, 377 (1993).
- [77] I. Bombaci and U. Lombardo, *Phys. Rev. C* **44**, 1892 (1991).
- [78] L. Lindblom, *Astrophys. J.* **278**, 364 (1984).
- [79] N. K. Glendenning, *Phys. Rev. D* **46**, 4161 (1992).